

Constraints on Neutrino Masses from Weak Lensing

Kiyotomo Ichiki^{1,2*}, Masahiro Takada^{3†}, Tomo Takahashi^{4‡}

¹*Department of Physics and Astrophysics, Nagoya University, Nagoya 464-8602, Japan*

²*Research Center for the Early Universe, University of Tokyo, Tokyo 113-0033, Japan*

³*Institute for the Physics and Mathematics of the Universe (IPMU),
The University of Tokyo, Chiba 277-8582, Japan and*

⁴*Department of Physics, Saga University, Saga 840-8502, Japan*

(Dated: December 3, 2018)

The weak lensing (WL) distortions of distant galaxy images are sensitive to neutrino masses by probing the suppression effect on clustering strengths of total matter in large-scale structure. We use the latest measurement of WL correlations, the CFHTLS data, to explore constraints on neutrino masses. We find that, while the WL data alone cannot place a stringent limit on neutrino masses due to parameter degeneracies, the constraint can be significantly improved when combined with other cosmological probes, the WMAP 5-year (WMAP5) data and the distance measurements of type-Ia supernovae (SNe) and baryon acoustic oscillations (BAO). The upper bounds on the sum of neutrino masses are $\sum m_\nu = 1.1, 0.76$ and 0.54 eV (95% CL) for WL+WMAP5, WMAP5+SNe+BAO, and WL+WMAP5+SNe+BAO, respectively, assuming a flat Λ CDM model with finite-mass neutrinos. In deriving these constraints, our analysis includes the non-Gaussian covariances of the WL correlation functions to properly take into account significant correlations between different angles.

PACS numbers: 04.50.+h, 98.80.Cq, 98.80.-k

I. INTRODUCTION

There are growing evidences that neutrinos have finite masses. The atmospheric, solar, reactor and accelerator neutrino oscillation experiments have confirmed that at least two of the three neutrino species have finite masses and their mass differences obtained from current experiments are $|\Delta m_{21}^2| \approx 7.7 \times 10^{-5} \text{ eV}^2$ and $|\Delta m_{31}^2| \approx 2.4 \times 10^{-3} \text{ eV}^2$ [1]. However, the absolute mass scale has yet to be determined because these experiments are only sensitive to the mass differences. Whereas kinematical probes such as tritium beta decay experiments and neutrinoless double beta decay experiments give upper bounds on the absolute neutrino mass [2, 3, 4], cosmological observations provide a powerful, albeit indirect, means of constraining neutrino properties, indeed yielding a more stringent upper bound on the total neutrino mass at present.

The finite-mass neutrinos affect structure formation via their effects on cosmic expansion history as well as on the evolution of perturbations in structure formation, which imprint characteristic signatures onto the cosmic microwave background (CMB) anisotropies and the mass clustering history in large-scale structure at low redshifts (see [5] for a thorough review). In particular the neutrinos slow down the growth of total matter clustering compared to a pure cold dark matter (CDM) model, because the neutrinos with large thermal velocities cannot be trapped by the gravitational potential well due to CDM inhomogeneities on small scales – the free-streaming effect [6]. Combining the CMB information with low-redshift cosmological probes allows to efficiently track the suppression effect on gravitational clustering during the matter-radiation equality and low redshifts [7, 8]. In fact, with the advent of high-precision cosmological probes, extensive efforts have been made in order to derive a stringent upper limit on neutrino masses by using/combining CMB and clustering properties of galaxies and Lyman- α forests [9, 10, 11, 12, 13, 14, 15, 16, 17].

There is another vital probe of mass clustering: weak lensing (WL) or the so-called cosmic shear, the bending of light by intervening mass distribution that causes images of distant galaxies to be distorted (see [18] for a thorough review). These sheared source galaxies are mostly too weakly distorted to measure the effect on single galaxies, however, the lensing signals are measurable by correlating the different galaxy images – the shear correlation functions. The weak lensing probes the distribution of total matter along the line of sight, i.e. this method is free of galaxy bias uncertainties. Various groups have measured the weak lensing correlations and have also used the measurements to constrain cosmological models since the first detections [19, 20, 21, 22]. Moreover there are several studies that assess the ability of future lensing surveys to constrain the neutrino masses [23, 24, 25, 26]. However, the actual use of WL measurements for constraining the neutrino masses has not been explored yet.

* E-mail address: ichiki@a.phys.nagoya-u.ac.jp

† E-mail address: masahiro.takada@ipmu.jp

‡ E-mail address: tomot@cc.saga-u.ac.jp

In this paper, therefore, we pursue a new constraint on neutrino masses by using the latest WL data set, the Canada-France-Hawaii Telescope Legacy Survey (CFHTLS) [27], and also by combining it with other cosmological probes, the WMAP 5-year data, [28], the type Ia supernova data [29], and the baryon acoustic oscillation experiment [30]. For this purpose, it is critically important to take into account the covariances of the WL correlation functions used, because there are significant cross-correlations between the WL correlations of different angles – the off-diagonal terms of the covariances are non-vanishing even for a pure Gaussian field. We use the halo model approach developed in [31] to compute the covariances, and also discuss the effect of a possible uncertainty in the covariance estimation on the final neutrino constraint.

The paper is organized as follows. In Section II-A we define the WL correlation functions in terms of cosmological parameters and discuss how finite-mass neutrinos affect the WL signals. In Section II-B we describe our model to compute the covariances of the WL correlation functions. After giving a brief description of other cosmological probes (CMB, SNe and BAO) in Section II-D, we show the main results for the neutrino mass constraints in Section III. Section IV is devoted to conclusions.

II. METHODOLOGY

A. Preliminary

In this section we briefly review how cosmic shear observable is related to cosmology, with particular attention to the effect of finite-mass neutrinos on cosmic shear.

The cosmic shear field is the weighted mass distribution integrated along the line of sight. The cosmic shear fields are measurable only in a statistical sense. A most conventional method used in the literature is the two-point correlation based methods such as the two-point correlations of the shear field. The Fourier transformed counterpart is the shear power spectrum, P_κ , which is obtained by projecting the 3D matter power spectrum, $P_\delta(k)$, weighted with the lensing kernel:

$$P_\kappa(\ell) = \frac{9H_0^4\Omega_m^2}{4c^2} \int_0^{\chi_H} \frac{d\chi}{a^2(\chi)} P_\delta \left(k = \frac{\ell}{f_K(\chi)}; \chi \right) \times \left[\int_\chi^{\chi_H} d\chi' n(z) \frac{dz}{d\chi'} \frac{f_K(\chi' - \chi)}{f_K(\chi')} \right]^2, \quad (1)$$

where χ is the comoving distance along the light ray, χ_H is the distance to the Hubble horizon, ℓ is the 2D wavevector perpendicular to the line of sight, $H_0 = 100h \text{ km s}^{-1} \text{ Mpc}^{-1}$ is the Hubble constant, and $f_K(\chi)$ is the comoving angular diameter distance out to a distance χ . Note that in practice χ_H is taken to be the comoving distance out to a redshift where a source galaxy distribution is sufficiently decaying. The function $n(z)$ is the redshift distribution of source galaxies, for which we adopt the following form characterized by three parameters according to [27]:

$$n(z) = \frac{\beta}{z_s \Gamma\left(\frac{1+\alpha}{\beta}\right)} \left(\frac{z}{z_s}\right)^\alpha \exp\left[-\left(\frac{z}{z_s}\right)^\beta\right], \quad (2)$$

where $\Gamma(x)$ is the Gamma function. Note that $n(z)$ is normalized so as to satisfy the condition $\int_0^\infty dz n(z) = 1$. The parameters α , β , and z_s are calibrated by using the CFHT Deep Fields and the VIRMOS VLT Deep Survey [32]. Because the uncertainties in parameters α and β are small they were fixed to 0.838 and 3.43, respectively, while the parameter z_s will be marginalized over assuming a Gaussian prior in the following analysis: $z_s = 1.172 \pm 0.026$, as was done in [33]. For $l \gtrsim 100$ the major contribution to $P_\kappa(l)$ comes from nonlinear clustering (e.g., see Fig. 2 in [34]). As described below, we employ the fitting formula in [35] to compute the nonlinear $P_\delta(k)$ from the input linear matter power spectrum. For the calculation of the linear matter spectrum, we use the CAMB code [36] up to the wavenumber $k \leq k_{\text{split}} = 25 \text{ Mpc}^{-1}$, and small scale solutions of Hu & Eisenstein [37] for $k \geq k_{\text{split}}$. We chose this wavenumber because the bulk of information in WL comes from wavenumbers up to $k/h \sim 1 \text{ Mpc}^{-1}$ [38]. We confirmed that the results are stable against the change of k_{split} .

The formulae to map the linear matter power spectra to the nonlinear ones have been derived and tested against N -body simulations for CDM cosmologies. For a mixed dark matter model, the nonlinear matter power spectrum has yet to be understood, except for the initial attempts to study the weakly nonlinear regime of gravitational clustering based on the perturbation theory [39, 40] and the hybrid N -body simulation [41]. In this paper we employ a similar prescription to that developed in [39] (also see [26]) in order to compute the nonlinear power spectrum for a mixed dark matter model. Our method is as follows. First, recall that, for a range of neutrino masses of interest, the finite mass neutrinos have large free-streaming scale below which the density perturbation of neutrinos is negligible; $k_{\text{fs}} \sim 0.04(m_\nu/0.1 \text{ eV})(\Omega_{\text{m}0}/0.27)^{1/2} h\text{Mpc}^{-1}$ (see Appendix A in [8] for the details), where $\Omega_{\text{m}0}$ is the present-day

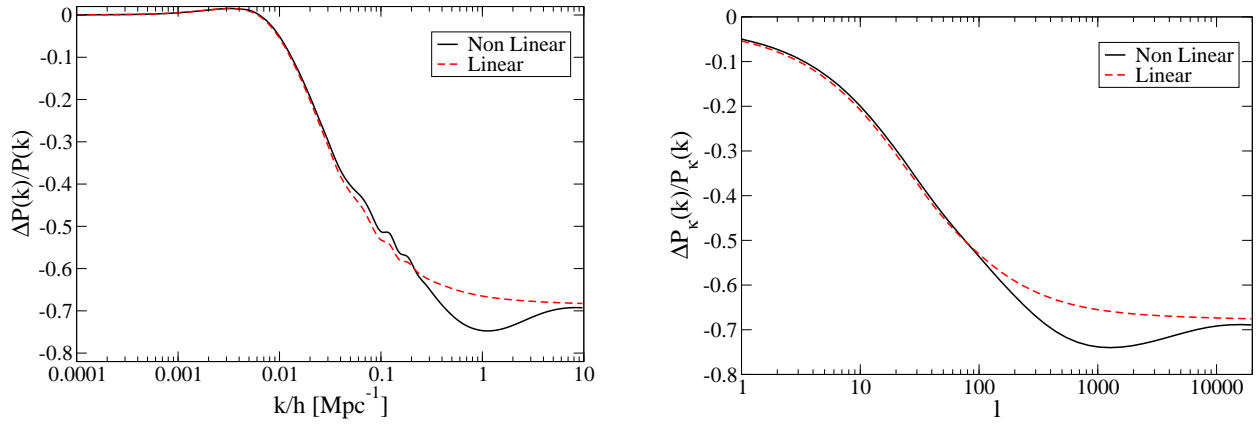


FIG. 1: *Left panel:* A fractional difference between the matter power spectra for a concordance Λ CDM model ($\Omega_{m0} = 0.3$) and a model with finite-mass neutrinos ($\Omega_{cb0} = 0.27$ and $\Omega_{\nu0} = 0.03$). Note that the total matter density $\Omega_{m0} (= \Omega_{cb0} + \Omega_{\nu0})$ and other cosmological parameters are fixed for the two models. The solid curve shows the model prediction including the correction of nonlinear mass clustering (see the text for the details), while the dashed curve shows the linear-theory prediction. The finite-mass neutrinos cause a suppression in the power spectrum amplitudes on scales below the free-streaming scale. The suppression effect is enhanced over transition scales between linear and nonlinear regimes. *Right panel:* A similar plot, but for the lensing power spectrum as a function of multipoles l .

energy density of total matter in units of the critical density. Hence we assume that the neutrino density perturbations stay in the linear regime, which can be precisely computed by solving the hierarchical Boltzmann equations coupled to the Einstein equations using the CAMB. On the other hands, the nonlinear clustering is driven mainly by the density perturbations of CDM plus baryon. In this setting, the density perturbation of total matter (CDM, baryon and neutrinos), which generates the gravitational potential causing gravitational lensing via the Poisson equation, is given as

$$\delta_{\text{tot}} = \frac{\delta\rho_c + \delta\rho_b + \delta\rho_\nu}{\bar{\rho}_c + \bar{\rho}_b + \bar{\rho}_\nu} = f_{\text{cb}}\delta_{\text{cb}} + f_\nu\delta_\nu^{\text{L}}, \quad (3)$$

where

$$f_{\text{cb}} \equiv \frac{\Omega_{c0} + \Omega_{b0}}{\Omega_{m0}}, \quad f_\nu \equiv \frac{\Omega_{\nu0}}{\Omega_{m0}}, \quad \delta_{\text{cb}} \equiv \frac{\delta\rho_{\text{cb}} + \delta\rho_b}{\bar{\rho}_c + \bar{\rho}_b}. \quad (4)$$

The subscripts ‘c’, ‘b’, ‘ ν ’ and ‘cb’ stand for CDM, baryon, finite mass neutrinos, and CDM plus baryon, respectively, Ω_{i0} ($i = c, b$ and so on) denotes the present-day energy density of the i -th component, f_i is its fractional contribution to the total energy density, and δ_ν^{L} represents the linear density perturbation of neutrinos. Note that $f_{\text{cb}} + f_\nu = 1$. We neglect the gravitational dragging force on nonlinear density perturbations of baryon and CDM from neutrinos. As stated above, we use the mapping formula of [35] to compute the nonlinear density perturbation of CDM plus baryon from the input linear one. Then the nonlinear power spectrum of total matter is given by

$$P_\delta^{\text{NL}}(k) = \langle \delta_{\text{tot}}^2 \rangle = f_\nu^2 \langle (\delta_\nu^{\text{L}})^2 \rangle + f_{\text{cb}}^2 \langle (\delta_{\text{cb}}^{\text{NL}})^2 \rangle + 2f_\nu f_{\text{cb}} \langle \delta_\nu^{\text{L}} \delta_{\text{cb}}^{\text{NL}} \rangle, \quad (5)$$

where we have introduced the superscript ‘NL’ to explicitly state the quantities in the nonlinear regime. The sensitivity of the nonlinear power spectrum depends to neutrino masses arises from the growth rate in each density perturbations as well as from the dependence of each terms in Eqn. (5) on f_ν .

One may imagine a more crude approach that the nonlinear power spectrum is mapped by inserting the input linear power spectrum of total matter into the fitting formula treating the total matter as a single fluid. We have checked that the result obtained in this approach is not so largely different from our fiducial approach of Eqn. (5) as long as neutrino masses are small. Even so we believe that the method above is more sensible in a sense that the method includes the perturbation theory result [39] when the perturbations are in the weakly nonlinear regime.

The effect of finite mass neutrinos on $P_\delta^{\text{NL}}(k)$ is depicted in the left panel of Fig. 1, showing the relative difference between the nonlinear power spectra with and without finite mass neutrinos, where Ω_{m0} is kept fixed. For comparison the corresponding result for the linear power spectra is also shown, where the denominator and numerator in $\Delta P_\delta/P_\delta$ are both the linear spectra. On very large distance scales (i.e. very small k), well beyond the neutrino free-streaming scale, the neutrino effect is absent, as the neutrinos can cluster together with the CDM plus baryon perturbations.

For intermediate scales, corresponding to $k \simeq [0.01 - 0.1]h\text{Mpc}^{-1}$ for the case with $m_\nu \sim 0.5 \text{ eV}$, the neutrinos cause a characteristic scale-dependent suppression in the matter power spectrum amplitude. Very interestingly, the neutrino suppression effect is enhanced on scales around $k \sim 1h\text{Mpc}^{-1}$ compared to the linear theory prediction, which is consistent with the perturbation theory result found in [39]. Perhaps even more surprisingly, the amount of the neutrino suppression effect becomes similar to that of the linear theory prediction on the smaller scales $k \gtrsim 1h\text{Mpc}^{-1}$, well below the free-streaming scale. That is, the neutrino effect appears just as a constant offset in the overall amplitude on the small scales, even though the power spectrum amplitude itself is significantly boosted in the nonlinear regime compared with the linear theory. This seems consistent with the result indicated by the hybrid N -body simulations [41], although the simulation resolution may be insufficient to follow this nonlinear regime. The amount of neutrino suppression on scales down to nonlinear regime is roughly given by $\Delta P_\delta/P_\delta \sim -8f_\nu$ which is sensitive to total neutrino mass as $f_\nu \simeq \sum m_\nu/[\Omega_{\text{m}0}h^2(94.1 \text{ eV})]$, but not sensitive to the mass scale of individual neutrinos.

There is a good rationale to believe that our modeling of the nonlinear power spectrum is fairly reasonable according to the previous findings in the literature. As accounted for in the fitting formula [35], the nonlinear spectrum amplitude at a given scale is very sensitive to the local amplitude as well as the local spectral slope $n_{\text{eff}} = d \ln P_\delta^L / d \ln k$ of the input linear power spectrum at that scale, where the power spectrum is a decreasing function with increasing k at relevant nonlinear scales (also see [42]). In particular a change in the local spectral slope induces a scale-dependent modification in the shape of the nonlinear power spectrum over a range of the transition scales between the linear and nonlinear regimes (also see Fig. 1 in [42]). Having in mind these properties, the result in Fig. 1 for the input linear power spectra explicitly shows that including finite-mass neutrinos leads to a change in the local spectral slope over a range of the intermediate scales, causing the enhanced neutrino effect in the weakly nonlinear regime. On very small scales, the local spectral slope is unchanged, therefore, the neutrino effect becomes scale-independent.

Thus the finite mass neutrinos affect the lensing power spectrum via the effect on the matter power spectrum, even for a fixed $\Omega_{\text{m}0}$, which keeps the lensing efficiency function unchanged. The right panel of Fig. 1 shows the neutrino effect on the lensing spectra. The neutrinos suppress the lensing spectrum amplitudes over all the angular scales probed by the current data. Note that the baryon oscillation wiggles are completely washed out due to the projection. Thus, since the shear correlation function is a Fourier-transform of the lensing power spectrum, the neutrino effect can be potentially extracted from the measured shear correlations. In particular, if we can use the small angular scales with a robust model prediction, the accuracy of constraining neutrino masses can be significantly improved in the nonlinear regime compared to the linear regime, due to the increased signal-to-noise ratio by the boosted amplitudes of shear correlations.

B. The CFHTLS result for cosmic shear measurement

The data we will use to put limits on neutrino masses is taken from the latest Canada-France-Hawaii Telescope Legacy Survey (CFHTLS or we will often call WL for simplicity) [27]. It covers over 57 square degrees, which drops to the effective area of 34.2 square degrees after taking into account the masking corrections of the surveyed region, and comprises about 1.7×10^6 galaxies whose shapes were used for the lensing shear correlation analysis. In their paper, the shear correlation is given in terms of correlation function ξ , γ , and M_{ap} , all of which are related to the same convergence power spectrum (Eqn. [1]) with different filtering. They found that these three statistics give consistent results on cosmological parameter estimations. In this paper we therefore use one of the correlation functions, ξ .

It is useful to decompose the cosmic shear correlations into the E (irrotational) and B (rotational) mode contributions, because the cosmological shear field creates the E -mode field alone. The E -mode correlation ξ_E is related to the convergence power spectrum P_κ [43, 44, 45] as

$$\xi_E(\theta) = \int_0^\infty \frac{\ell d\ell}{2\pi} P_\kappa(\ell) J_0(\ell\theta), \quad (6)$$

where θ is the separation angle between galaxy pairs, and J_0 is the zero-th order Bessel function. In practice, since the shear power spectrum is difficult to measure due to the complex survey geometry, the E -mode correlation function is estimated from the measured correlation functions $\xi_\pm(\theta)$ as proposed in [43]:

$$\xi_E(\theta) = \frac{1}{2} \left[\xi_+(\theta) + \xi_-(\theta) + \int_\theta^\infty \frac{d\theta'}{\theta'} \xi_-(\theta') \left(4 - 12 \frac{\theta^2}{\theta'^2} \right) \right], \quad (7)$$

where $\xi_\pm(\theta)$ is the two-point correlations of ellipticities between paired galaxies separated by angle θ ; the ‘+’ component is the tangential or radial ellipticity component with respect to the line connecting the two galaxies, while the component ‘×’ is its 45 degree rotated component. Thus, the transformation relation of ξ_E from the measured $\xi_\pm(\theta)$ includes an integration of ξ_- up to an infinite separation $\theta \rightarrow \infty$. However, in practice, ξ_E needs to be estimated from

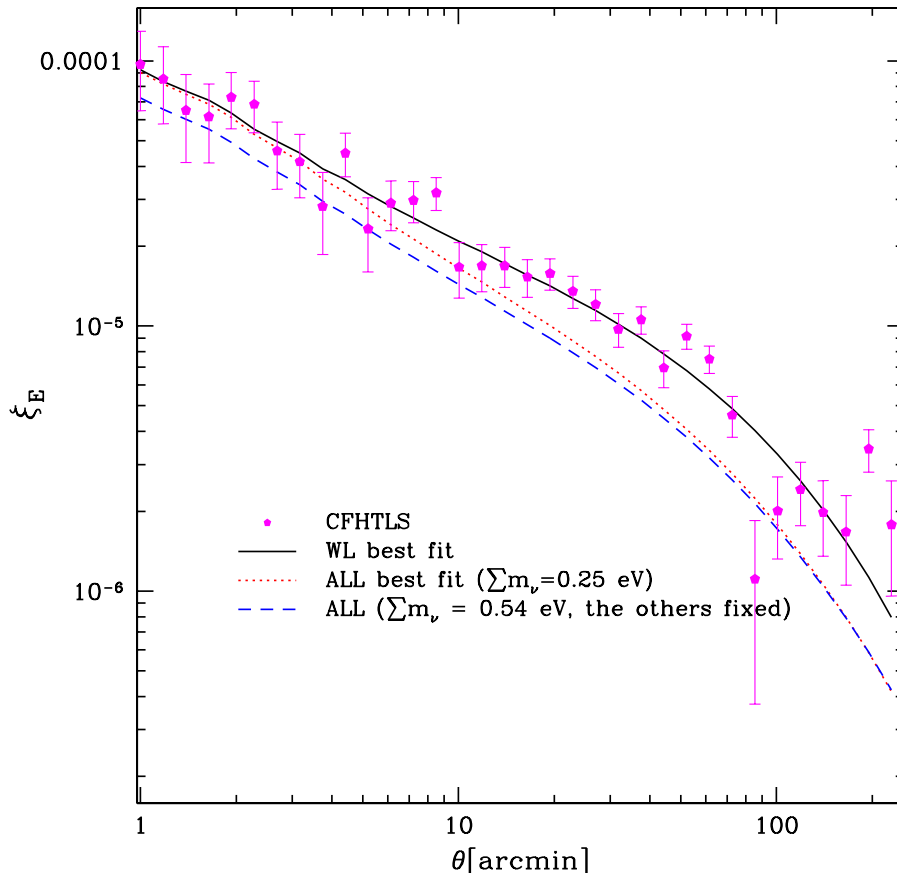


FIG. 2: The data points show the measured shear correlation functions, $\xi_E(\theta)$, at each angular bins, which are taken from the CFHTLS result in [27]. The error bars around each data points are computed from diagonal terms in the inverse of the covariance matrix that includes contributions from the shot noise of intrinsic galaxy ellipticities and the Gaussian and non-Gaussian sample variances (see the text for the details). The solid curve is the model prediction for the Λ CDM model with finite-mass neutrinos which best matches the WL measurement. The dotted curve is the best-fitting model prediction for the joint fitting of WL+WMAP5+SNe+BAO as will be shown below. Note that the best-fitting model has the total neutrino mass of $\sum m_\nu = 0.25$ eV. To demonstrate the effect of finite-mass neutrinos on ξ_E , the dashed curve shows the model prediction where the neutrino mass is changed to $\sum m_\nu = 0.54$ eV, roughly at two sigma upper bound for the joint fitting, and other cosmological parameters are fixed to their best-fitting values.

a finite range integration that may introduce a residual uncertainty in the estimated $\xi_E(\theta)$. We ignore this uncertainty in our paper for simplicity.

Fig. 2 shows the measured shear correlation function ξ_E taken from Table B.1 in [27], comparing with the model predictions which best fit to to the CFHT WL data and the case combined with the WMAP5 and other distance measurements (see below for the details). The error bars at each angular bins are computed from the diagonal components of the inverse of the covariance matrix, and the data points between different separation angles are significantly correlated to each other as described below in detail.

C. Covariances of shear correlation functions

The covariance matrix of shear correlation function quantifies (1) statistical uncertainties in measuring the shear correlation function at each angular bin, and (2) how the correlation functions of different angular bins are correlated with each other. Following the method in [31, 47] (more explicitly see Eqn. [29] in [31]), the covariance matrix of the

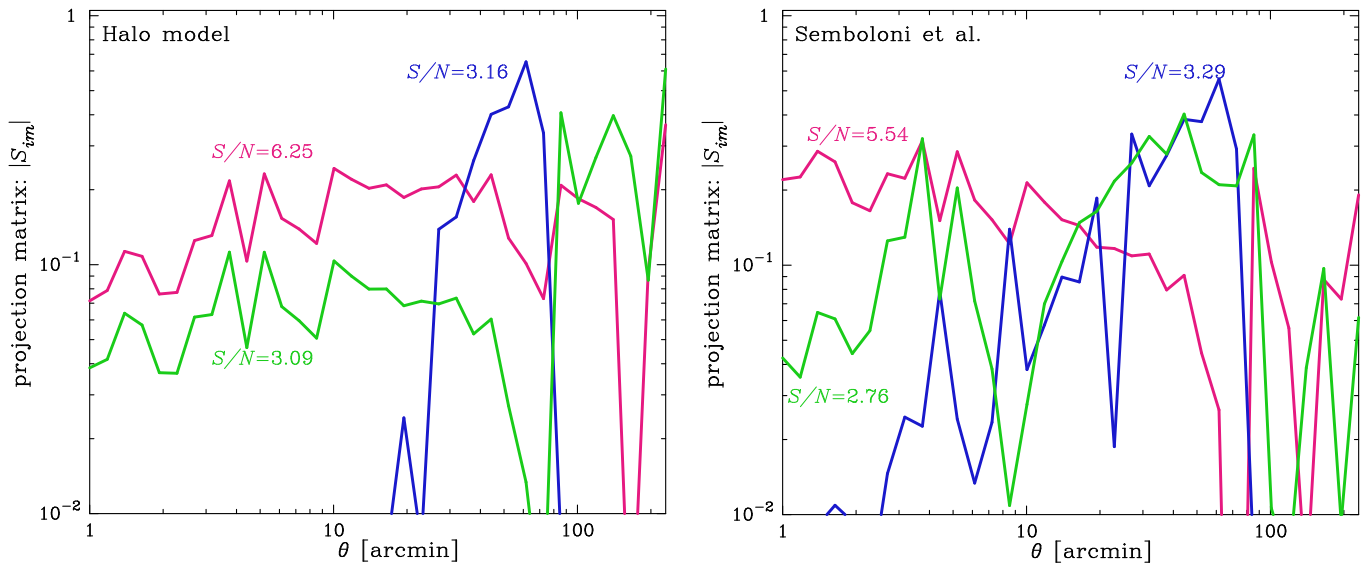


FIG. 3: The projection matrix $|S_{lm}|$ for the principal component decomposition of the normalized covariance matrix is plotted, for first three eigenmodes that have largest differential contributions to the cumulative signal-to-noise ratio, (S/N) , defined by Eqn.(9). The left panel shows the results obtained when using the halo model developed in [31] to compute the covariance matrix. The total signal-to-noise ratio $S/N = 10.6$. The right panel shows the result when the fitting formula in Semboloni et al. (2007) [46] is employed, yielding $(S/N) = 8.89$. For the real-space correlation function, the projection matrix for each eigenmodes has a broad tail, reflecting significant correlations between different angles. It is also found that the contributions from each separation angles become different depending on which model of the covariance matrix is used.

shear correlation function, \mathbf{C} , can be expressed as

$$\begin{aligned}
 [\mathbf{C}]_{ij} &\equiv \text{Cov}[\xi_E(\theta_i), \xi_E(\theta_j)] \\
 &= \delta_{ij}^K \text{Cov}_{\text{SN}} + \frac{1}{\pi A_s} \int_0^\infty l dl J_0(l\theta_i) J_0(l\theta_j) P_\kappa(l) + \frac{1}{4\pi^2 A_s} \int_0^\infty l dl \int_0^\infty l' dl' J_0(l\theta_i) J_0(l\theta_j) \bar{T}_\kappa(l, l'), \quad (8)
 \end{aligned}$$

where δ_{ij}^K denotes the Kronecker-type delta function defined so that $\delta_{ij}^K = 1$ when $\theta_i = \theta_j$ within the bin width, otherwise 0, A_s is the survey area in units of steradian and \bar{T}_κ is the angle averaged trispectrum of convergence. Note that the survey area is set to $A_s = 34.2$ square degrees as described above, and we have ignored the boundary and geometry effects of surveyed region for simplicity.

The first term on the r.h.s. of Eqn. (8), $\delta_{ij}^K \text{Cov}_{\text{SN}}$, denotes the the shot noise contamination due to intrinsic galaxy ellipticities, contributing only to the diagonal terms of the covariance matrix with $\theta_i = \theta_j$. The shot noise is determined by the rms intrinsic ellipticities and the total number of galaxy pairs that are available from the surveyed region in the separation angle of a given bin width. The shot noise can be estimated directly from the data: for example, since the coherent shear signals can be erased by randomly rotating each galaxy images by arbitrary angles, the shot noise contamination can be estimated from variations in the correlation functions that are repeatedly measured after randomization of galaxy image orientations. Our analysis uses the shot noise at each bin given in the column labeled as “ $\delta\xi_B$ ” in Table B1 of [27].

The second and third terms in Eqn. (8) denote the Gaussian and non-Gaussian sample variances, respectively, arising due to the imperfect sampling of shear correlations from a finite survey region. Since the lensing correlations probe the mass distribution in large-scale structure along the line of sight, modeling the sample variances requires a knowledge about the power spectrum and trispectrum of the 3D mass distribution, where non-Gaussian errors arise once the mass distribution probed by lensing resides in the nonlinear clustering regime. Thus the sample variances depend on the mass clustering strengths, i.e. on the underlying cosmology. There are several important features of these sample variances. First, contrary to the power spectrum covariance, the Gaussian term is non-vanishing for the off-diagonal components of the covariance when $\theta_i \neq \theta_j$: there are always correlations between the shear correlations of different angles. Second, the non-Gaussian sample variance contributes to both the diagonal and off-diagonal terms of the covariance matrix. The non-Gaussian errors become more significant on smaller angular scales where the lensing signals are more affected by the nonlinear regime.

Thus taking into account the covariance is critically important in order not to have too optimistic parameter estimation from the measured correlation functions. However, only a few previous works have studied the covariances

of cosmic shear correlations, based on ray-tracing simulations [46] and analytic methods [31, 47, 48]. In particular, the importance of non-Gaussian errors is not fully understood yet. In this paper, to estimate how an uncertainty in the covariance affects the results, we employ two models of the non-Gaussian covariances:

- (A) Compute the covariance matrix using the dark matter halo approach developed in [31].
- (B) Compute the non-Gaussian error contribution to the covariance by multiplying the fitting formula derived in [46] with each matrix elements of the Gaussian sample variance (the second term in Eqn.[8]).

For the first approach we also include sources of new non-Gaussian errors that inevitably arise for a *finite* survey area [49], although the new contribution seems not so significant as studied in [31]. Model A is our fiducial model to compute the covariance, but we will study how our results change when using Model B for the covariance evaluation. To compute the covariance we need to specify cosmological model, and our covariance evaluations assume the concordance Λ CDM model which is consistent with WMAP5.

It is useful to study how the two-point correlation functions of different separation angles are correlated with each other. To do this, we study the cumulative signal-to-noise (S/N) ratio for measuring the shear correlation functions. Using the normalized covariance matrix defined as $\tilde{C}_{ij} \equiv C_{ij}/[\xi_E(\theta_i)\xi_E(\theta_j)]$, the S/N is defined as

$$\left(\frac{S}{N}\right)^2 = \sum_{i,j=1}^{N_b} [\tilde{C}^{-1}]_{ij} = \sum_{m=1}^{N_b} \frac{1}{\lambda_m} \left(\sum_{i=1}^{N_b} S_{im} \right)^2, \quad (9)$$

where \tilde{C}^{-1} is the inverse matrix of \tilde{C} and N_b is the number of separation bins ($N_b = 34$ for CFHTLS as shown in Fig. 2). In the second equality we have used the principle component decomposition given as $\tilde{C}_{ij} = \sum_{m=1}^{N_b} S_{im} \lambda_m S_{jm}$, where λ_m is the m -th eigenmode and the projection matrix S_{im} describes how the i -th covariance element contributes to the m -th eigenmode. Note that the inverse matrix of \tilde{C} is given by $[\tilde{C}^{-1}]_{ij} = \sum_{m=1}^{N_b} S_{im}(1/\lambda_m)S_{jm}$, and the matrix S_{im} satisfies the conditions $\mathbf{S} = \mathbf{S}^T$, $\sum_{m=1}^{N_b} S_{im}S_{jm} = \delta_{ij}$, and $\sum_{m=1}^{N_b} (S_{im})^2 = 1$. Eqn. (9) expresses the S/N as a sum of the contributions from independent eigenmodes.

Fig. 3 shows the projection matrix of first three eigenmodes that have largest differential contributions to the $(S/N)^2$ in Eqn. (9), using either of the two models above to compute the covariance matrix. It is worth noting that Model A gives $S/N = 10.6$, while Model B gives $S/N = 8.89$, because Model B predicts more significant non-Gaussian errors than Model A as studied in [31]. For both the models, each projection matrix gives contributions over a wide range of separation angles, reflecting significant correlations between different angles. Thus there are fewer independent modes than the 34 bins of separation angles in Fig. 2: for both these two cases, first 15 eigenmodes give about 95% contribution to the $(S/N)^2$. Also note that the angular scales mainly contributing to the total S/N are different in these two models: for Model B based on the method in Semboloni et al. (2007), the small angular scales are more important in constraining cosmology.

We will use the log likelihood analysis to estimate cosmological parameter:

$$\ln \mathcal{L}^{\text{WL}} = -\frac{1}{2} \sum_{i,j=1}^{N_b} [\xi_E^{\text{obs}}(\theta_i) - \xi_E^{\text{model}}(\theta_i)] [\mathbf{C}^{-1}]_{ij} [\xi_E^{\text{obs}}(\theta_j) - \xi_E^{\text{model}}(\theta_j)], \quad (10)$$

where ξ_E^{obs} and ξ_E^{model} are the measured correlation function and the model prediction, respectively, and \mathbf{C}^{-1} is the inverse of the covariance matrix given as $[\mathbf{C}^{-1}]_{ij} = \xi_E(\theta_i)[\tilde{C}^{-1}]_{ij}\xi_E(\theta_j)$.

D. Likelihood analysis

Our likelihood analysis includes a fairly broad range of cosmological parameters that affect a Λ CDM cosmology with finite mass neutrinos. We will work on 8 parameters given as

$$\vec{p} = (\Omega_{b0}h^2, \Omega_{\text{dm}0}h^2, f_\nu, \theta_A, \tau, \ln(10^{10}\Delta_{\mathcal{R}}^2), n_s, z_s), \quad (11)$$

where θ_A is the so-called acoustic scale related to the distance to the last scattering surface [50], $\Omega_{\text{dm}0}h^2 \equiv (\Omega_{c0} + \Omega_{\nu 0})h^2$ stands for the dark matter density today, and $\Delta_{\mathcal{R}}^2$ and n_s are the amplitude and spectral index of the primordial curvature power spectrum defined at $k = 0.002 \text{ Mpc}^{-1}$ [11], respectively. The parameter space we explore in the following is: $\Omega_{b0}h^2 = [0.005, 0.1]$, $\Omega_{\text{dm}0}h^2 = [0.01, 0.99]$, $f_\nu = [0, 0.9]$, $\theta_A = [0.3, 10]$, $\tau = [0.01, 0.8]$, $\ln 10^{10}\Delta_{\mathcal{R}}^2 = [0.5, 6.0]$, $n_s = [0.5, 1.5]$, $z_s = [0.9, 1.4]$. Throughout this paper we assume the standard three flavor neutrinos that are

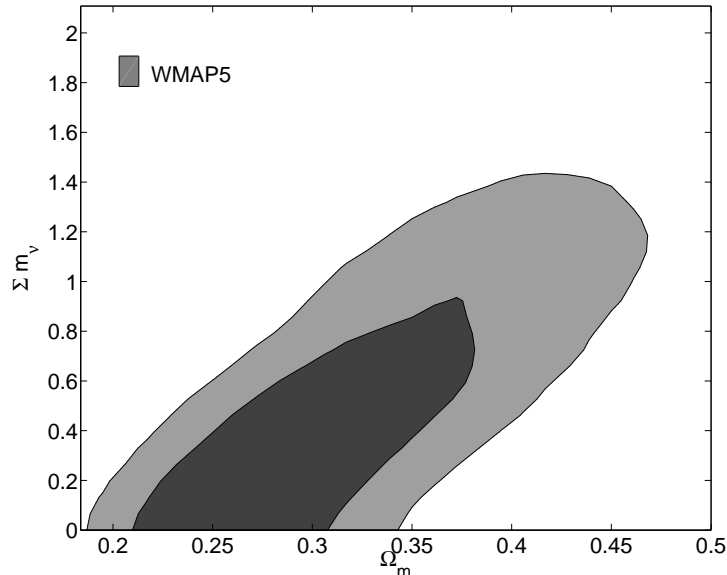


FIG. 4: The contours show the marginalized constraints (68% and 95% CL) for the $(\sum m_\nu, \Omega_{m0})$ -subspace, obtained by fitting the WMAP5 data to the Λ CDM model with finite-mass neutrinos.

completely degenerate in mass. Note that the parameter z_s specifies the galaxy redshift distribution that is needed to predict the shear correlation functions as described below Eqn. (2), and does not affect other cosmological probes such as WMAP5, SNe and BAO. Assuming flat priors for the cosmological parameters except z_s , we employ the MCMC method [51] to explore cosmological parameter estimations in the multi-dimensional parameter space given cosmological observables. For each run four parallel chains were computed and the convergence test was made based on the Gelman and Rubin statistics (“ $R-1$ ” statistics [52]). Our chains have typically 40000 points and $R-1 \lesssim 0.05$. In what follows we mention other cosmological probes used in our likelihood analysis, which adds complementary information to the cosmic shear data.

1. CMB

The CMB anisotropies are generated mainly until epochs before the last scattering surface of the decoupling epoch, $z \sim 1089$. Hence, if neutrino species are massive enough as $m_\nu \gtrsim 0.5$ eV (or $\sum m_\nu \gtrsim 1.5$ eV), they became non-relativistic before the recombination epoch [9]. In this case, the finite-mass neutrino causes a significant effect on the CMB spectrum mainly in two ways. First, for a fixed energy density of total matter (i.e. $\Omega_{m0} = \Omega_{cb0} + \Omega_{\nu0}$ fixed), the matter-radiation equality is delayed by the presence of finite-mass neutrinos. Hence this makes the heights of acoustic peaks higher, especially that of the first peak, in the CMB spectrum due to a greater early integrated Sachs-Wolfe effect. Second, the neutrinos cause an additional decay of the gravitational potential on small scales. This effect boosts the amplitudes of acoustic oscillations at higher multipoles through the dilation effect due to diminishing gravitational potential [53]. Through these effects, a precise measurement of the CMB spectrum can be used to place a limit on neutrino masses. In this paper we use the WMAP 5-year (WMAP5) data, and explore the likelihood which can be evaluated by the code publicly available at LAMBDA web site [64].

For the masses below $m_\nu \lesssim 0.5$ eV ($\sum m_\nu \lesssim 1.5$ eV), the neutrinos affect the CMB spectrum mainly through the effect on the angular diameter distance out to the last-scattering surface. In this case the effect is degenerate with other cosmological parameters such as Ω_{m0} and h [9]. Thus other cosmological probes complementary to CMB are needed to break the parameter degeneracies in order to explore the small mass scales of neutrinos.

2. Type Ia SNe

The distant type Ia supernovae (SNe) are one of such probes. The use of SNe as a standard candle allows us to estimate the luminosity distance - redshift relation. The estimated distance, more precisely the distance modulus, can be compared with a model prediction for a flat Λ CDM model with finite-mass neutrino contribution:

$$D_L(z) = \frac{c(1+z)}{H_0} \int_0^z dz' [\Omega_{r0}(1+z')^4 + \Omega_{cb0}(1+z')^3 + \Omega_\nu(z') + \Omega_{\Lambda0}]^{-1/2}, \quad (12)$$

where Ω_{r0} and $\Omega_{\Lambda0}$ are the energy densities of photon and cosmological constant, respectively, $\Omega_{\Lambda0} \approx 1 - \Omega_{m0}$ for a flat universe, and $\Omega_\nu(z)$ is the energy density at a redshift z . The contribution from radiation is negligible for the luminosity distance out to SNe at $z \lesssim 2$. In addition, since the current cosmological probes are only sensitive to neutrino masses greater than $\sim 0.1\text{eV}$ as will be shown below, neutrinos in this mass scale behave as non-relativistic matter over the redshift range of SNe data. Therefore, if we restrict our attention to a flat Λ CDM universe, the measured distance modulus of SNe constrain the information mainly on the total matter density Ω_{m0} . We use the latest compilation of SNe data set given by [29]. The SNe catalog provided consists of 307 SNe and is carefully calibrated taking into account various sources of the systematic errors.

3. BAO

Baryon acoustic oscillation (BAO) offers another probe. CMB measures the acoustic oscillations in the primordial photon-baryon plasma, which can be used to derive the angular diameter distance to the last scattering epoch, $z \approx 1089$. The same oscillation feature is imprinted onto the late-time matter power spectrum probed by a massive galaxy survey [54, 55]. This baryon acoustic oscillation feature therefore provides a standard ruler by which one can measure the distance to the redshift where the bulk of galaxies are observed. Eisenstein et al. [30] analyzed galaxies from Sloan Digital Sky Survey (SDSS) and provided their result in a form of an effective distance measure by averaging the distances in the radial and transverse directions:

$$D_V(z) = \left[(1+z)^2 D_A^2(z) \frac{cz}{H(z)} \right]^{1/3}, \quad (13)$$

where $D_A(z)$ is the angular diameter distance to the redshift $z = 0.35$. In this paper we use the following constraint on the distance parameter A provided in [30]:

$$A(z = 0.35) \equiv D_V(0.35) \frac{\sqrt{\Omega_{m0} H_0^2}}{0.35c} = 0.469 \left(\frac{n_s}{0.98} \right)^{-0.35} \pm 0.017. \quad (14)$$

Notice that the value of A is primarily sensitive to Ω_{m0} for a flat universe case.

III. RESULT AND DISCUSSION

A. Parameter constraints

The WMAP team reported an upper limit on the total neutrino mass, $\sum m_\nu < 1.3\text{eV}$ (95%CL), for a flat Λ CDM model plus one additional parameter of the total neutrino mass [11]. Using the same likelihood function given by WMAP team, we find a consistent but slightly tighter limit, $\sum m_\nu < 1.2\text{eV}$. This difference would be attributed to differences in the treatment of cosmological parameters as well as the priors between ours and WMAP5. In fact, we have found the consistent result if the same parametrization is adopted as theirs. In any case, these upper bounds are fairly close to the critical value $\sim 1.5\text{eV}$ as discussed in the previous section.

Fig. 4 shows the results we obtained from the WMAP5 data: the inner and outer contours show the 68% and 95% confidence level regions in the $(\Omega_{m0}, \sum m_\nu)$ -subspace, marginalized over other parameters. The contours show a strong degeneracy between these two parameters, reflecting that the CMB constraints come mainly from the effect of finite-mass neutrinos on the matter-radiation equality. The delay in the matter-radiation equality caused by the presence of massive neutrinos is compensated by adding more non-relativistic matter at present, i.e. increasing Ω_{m0} .

The results in Fig. 4 are not so encouraging from the perspective of complementarity between CMB and WL, because the WL constraints on the parameters Ω_{m0} and $\sum m_\nu$ are expected to show a similar degeneracy curve.

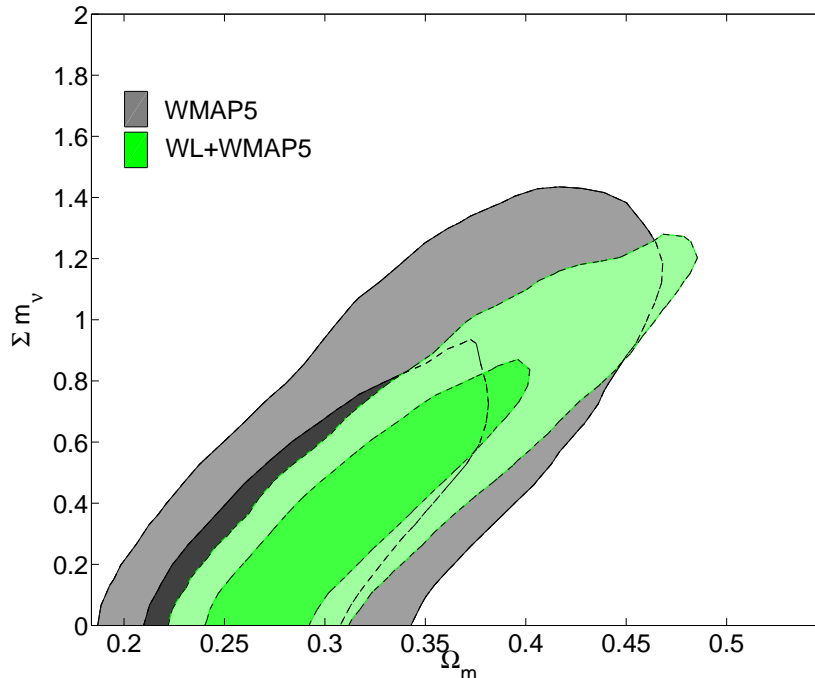


FIG. 5: The improvement in parameter constraints for $(\Omega_{m0}, \Sigma m_\nu)$ obtained by combining the CFHT WL data with WMAP5 (green-color contours), in comparison with the constraints for WMAP5 alone (black). The accuracy of Ω_{m0} determination is improved by adding the WL constraint, because the WL amplitude is sensitive to Ω_{m0} as can be found from Eqn. (1). However, the constraint on Σm_ν remains almost unchanged due to parameter degeneracies in the WL information.

The finite-mass neutrinos cause suppression in the amplitudes of cosmic shear correlations on relevant angular scales, however, this effect is compensated by increasing Ω_{m0} and/or the power spectrum normalization (see Fig. 1 and Eqn. [1]). Even so, since the degeneracy curves of CMB and WL constraints are not elongated to exactly the same direction, combining these two can always improve the constraints to some extent if they are consistent with each other.

Fig. 5 shows the constraints on the $(\Omega_{m0}, \Sigma m_\nu)$ -plane obtained when combining WMAP5 with the CFHT WL constraints. As expected from the above argument, the constraint is only slightly improved when the WL data is included. The upper bound on the total neutrino mass is $\Sigma m_\nu \lesssim 1.1$ eV for WL+WMAP5 compared to $\Sigma m_\nu \lesssim 1.2$ eV for WMAP5 alone. The reason why the constraint is not significantly improved is also attributed to the quality of WL data: the current WL data with ~ 30 square degrees is not so powerful yet compared to the WMAP5 data. Finally, the weak lensing data itself suffers from a strong degeneracy between Ω_{m0} and the power spectrum normalization, e.g. the Ω_{m0} - σ_8 degeneracy, as shown in [27]: adding the WL data cannot yet much break the degeneracy between Σm_ν and Ω_{m0} in the WMAP5 constraints.

Since the geometrical probes such as SNe and BAO are sensitive to Ω_{m0} for a flat Λ CDM model, by adding these probes into the WMAP5 and WL data, the constraint on neutrino masses can be further improved. In fact the WMAP team nicely demonstrated that combining SNe and BAO with the WMAP5 information tightens an upper limit on the neutrino masses by a factor of 2, resulting in $\Sigma m_\nu < 0.67$ eV [11].

Our analysis also confirmed this trend, but gives a slightly less improved limit, $\Sigma m_\nu < 0.76$ eV, as shown in Fig. 6. The difference would be due to the fact that we are using different BAO constraint from that used by the WMAP team. The BAO constraint employed here was one derived in Eisenstein et al. [30] using the spectroscopic sample of the SDSS Luminous Red Galaxies (LRGs) that probes the distance out to $z = 0.35$. This BAO measurement has a less constraining power than that more recently derived by Percival et al. [56], which was used in the WMAP5 analysis. Since they used a bigger galaxy sample combining the SDSS LRGs with the SDSS main galaxy sample and the 2dF galaxy sample, which probe the distances to redshifts $z = 0.2$ and $z = 0.35$. The constraints from Percival et al. are more powerful than those from Eisenstein et al.; for example, Percival et al. constrain Ω_{m0} with the precision of $\Omega_{m0} = 0.249 \pm 0.018$ for a Λ CDM model, while Eisenstein et al. give $\Omega_{m0} = 0.273 \pm 0.025$. In addition, as indicated from Fig. 5, the smaller best-fitting value of Ω_{m0} prefers a smaller Σm_ν when the WMAP5 and BAO is combined.

However, a marginal tension between the two data sets of BAO has been discussed in the literature, which leads to a possible inconsistency for a Λ CDM model (e.g., see Fig. 12 in [11]). This tension is not found if the BAO distance of $z = 0.2$ is not included. For these reasons, we employ the BAO constraint by Eisenstein et al. to derive a conservative constraint on neutrino masses.

Fig. 6 shows how the neutrino mass constraints are improved when some or all of WMAP5, WL, BAO and SNe constraints are combined. Interestingly, adding the WL data into WMAP5+BAO+SNe does improve the constraint on the total neutrino mass, leading to the upper bound $\sum m_\nu < 0.54$ eV, because the degeneracy with Ω_{m0} is more efficiently broken. It is also worth noting that a most significant degeneracy inherent in the weak lensing constraints, the Ω_{m0} - σ_8 degeneracy, is efficiently broken by combining all the probes, as shown in Fig. 7. Our final results are $\Omega_{m0} = 0.294 \pm 0.02$ and $\sigma_8 = 0.758 \pm 0.03$, improved by a factor of 10 and 5 from the constraints by the WL data alone.

The shear correlation function for our best-fitting model is shown by the dashed curve in Fig. 2, in comparison with the measurement of WL and the model prediction (solid curve) that matches the WL data alone. The prediction of the best-fitting model to all the data combined (dotted curve) has systematically smaller amplitudes than the measurement data points, especially on large angular scales. However, it is worth noting that the change in χ^2 between the two best-fitting models for the joint fitting and the WL data alone is only $\Delta\chi_{\text{WL}}^2 \simeq 2$ due to significant correlations between the different data bins as implied in Fig. 3. Adding more massive neutrinos to the model with other parameters being fixed leads to further smaller WL amplitudes compared to the data. The dashed curve shows the result for such a model assuming $\sum m_\nu = 0.54$ eV, a mass scale at about 2σ upper limit for the joint fitting, whose χ^2 value differs from the dotted curve by $\Delta\chi_{\text{WL}}^2 \simeq 2$.

The marginalized constraints and likelihood distribution of individual parameters of interest are summarized in Table I and Fig. 8, respectively. The precisions of constraining some parameters such as Ω_{m0} , $\Omega_{\text{dm}0}h^2$, σ_8 and $\sum m_\nu$ are significantly improved when all the probes are combined.

TABLE I: Summary of the constraints on cosmological parameters and the marginalized errors for $\nu\Lambda$ CDM model

Parameter	WL	WL+WMAP5	WMAP5+SN+BAO	ALL
$\Omega_{\text{dm}0} h^2$	0.22 ± 0.09	0.12 ± 0.0065	0.11 ± 0.0038	0.11 ± 0.0030
H_0 [km s ⁻¹ Mpc ⁻¹]	74 ± 15	65 ± 3.9	68 ± 2.0	68 ± 1.9
n_s	1.0 ± 0.26	0.95 ± 0.016	0.96 ± 0.014	0.96 ± 0.014
$\ln(10^{10} \Delta_{\mathcal{R}}^2)$	2.8 ± 1.0	3.2 ± 0.046	3.2 ± 0.040	3.2 ± 0.039
$\sum m_\nu$ [eV]	< 8.1 (95% CL)	< 1.1	< 0.76	< 0.54
σ_8	0.64 ± 0.15	0.73 ± 0.045	0.73 ± 0.059	0.76 ± 0.033
Ω_{m0}	0.52 ± 0.20	0.33 ± 0.056	0.29 ± 0.021	0.29 ± 0.020

B. Discussion of systematic errors

There are several sources of systematic errors to affect weak lensing measurements. One of those is uncertainties in the source galaxy redshifts. As described in detail in [27], the redshift distribution of source galaxies is carefully calibrated by using secure photometric redshifts of the CFHT deep fields, in combination with the VIMORS spectroscopic sample, assuming that the deep fields contain a representative galaxy sample of the WL galaxies. We below estimate how a possible residual error in the source galaxy redshifts, reported in [27], affects our neutrino constraint. Since the amplitude of cosmic shear correlations is sensitive to mean redshift of galaxies, a most relevant parameter in the source galaxy distribution is the parameter z_s in Eqn. (2) for which we have so far assumed $z_s = 1.172 \pm 0.026$ for the fiducial value and the 1σ uncertainty. Note that we have also employed the Gaussian prior $\sigma(z_s) = 0.026$ around the central value in our MCMC analysis.

The left panel of Fig. 9 shows how the constraints on $\sum m_\nu$ and σ_8 change for the WL data combined with WMAP5 if we put a more restrictive prior on z_s by a factor of 2 or 4 than the fiducial prior. The effects appear to be small: the confidence regions shrink only slightly. This is simply because the uncertainty in z_s considered here is already sufficiently small compared with the statistical uncertainties in the shear correlation measurement.

The right panel of Fig. 9 shows how a shift in the central value of z_s causes a bias in the best-fitting cosmological parameters, assuming the fiducial prior $\sigma(z_s) = 0.026$. The smaller or larger source redshift gives larger or smaller best-fitting values of σ_8 , respectively (e.g., see [27, 57]), while the neutrino constraint is little affected. The effects of uncertainties in these parameters on cosmological constraints are found to be very small ($\sim 1\%$) in the present analysis. However, note that it will be of critical importance to have a precise knowledge on source galaxy redshifts

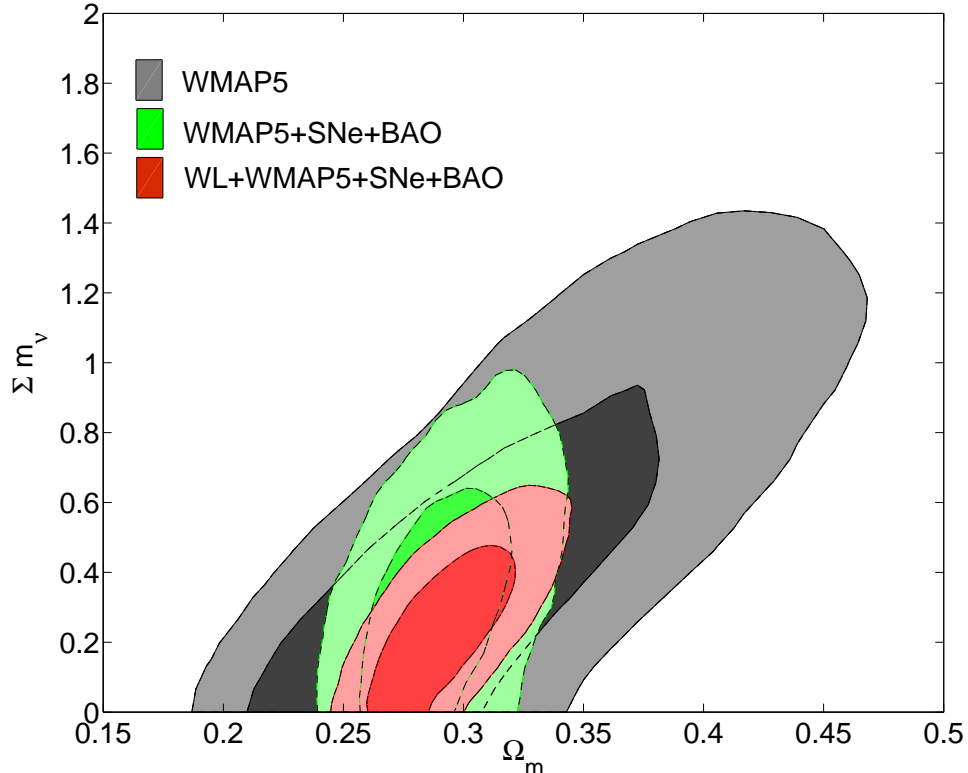


FIG. 6: Two-dimensional marginalized constraints on the neutrino mass $\sum m_\nu$ and Ω_{m0} are significantly improved when the constraints for WMAP5+WL are combined with the information from the geometrical probes, SNe and BAO. The black, green and red contours show the results for WMAP5, WMAP5+SNe+BAO, and WL+WMAP5+SNe+BAO, respectively. The marginalized upper bound on the neutrino mass is given as $\sum m_\nu \lesssim 0.54$ eV for all the probes combined.

especially when we have a sufficiently accurate measurement of cosmic shear that is more powerful in constraining neutrino masses than the CMB information [26].

As described in § II C, there is an uncertainty in estimating the sampling variance contributions to the covariance matrix of the shear correlation functions. We have so far used the halo model approach developed in [31] to compute the covariance matrix. Fig. 10 shows the constraints on $\sum m_\nu$ and Ω_{m0} obtained when using the different model for the covariance matrix evaluation, Model B based on [46]. These models are different in computing the non-Gaussian error contributions to the covariance. The confidence regions for Model B are enlarged compared to those for Model A. The best-fitting parameters are only slightly changed: $\sum m_\nu = 0.25$ and 0.21 for Model A and B, respectively. Model B predicts more significant non-Gaussian errors on angular scales of $\theta \lesssim 10$ arcminutes than Model A, i.e. stronger correlations between the shear correlation functions of different angular bins. The correlations reduce independent modes of the angular scales to be useful for constraining cosmology. This explains larger confidence regions for Model B. Also, as shown in Fig. 3, different angular scales of the shear correlation functions contribute to the cosmological constraints in a different way between Model A and B, causing a slight difference between the best-fitting parameters. Even so, it can be found that, thanks to a wide coverage of angular scales for the CFHT, the results for the two covariance models are consistent, implying that the large angular scales where the Gaussian errors are dominant in the covariance mainly contribute to the constraints on cosmological parameters.

There are other sources of systematic errors such as those inherent in the galaxy shape measurements. Estimating this effect is beyond the scope of our paper, so we do not discuss those effects here.

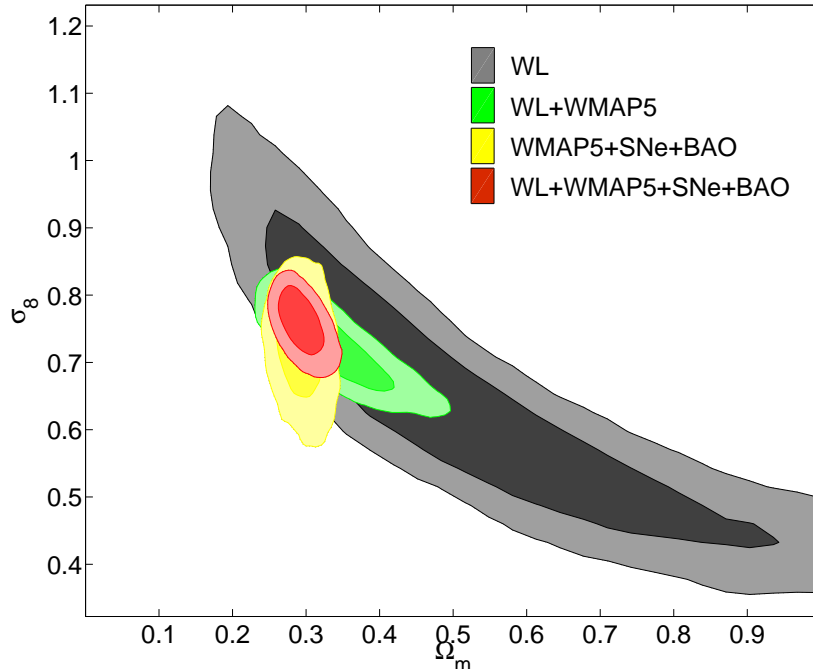


FIG. 7: Two-dimensional marginalized constraints on σ_8 and Ω_{m0} , for WL+WMAP5 (green) and WL+WMAP5+SN+BAO (red), respectively, in comparison with the constraints from WL alone (black). The yellow contours show the region from WMAP5+SN+BAO (without WL).

IV. CONCLUSION AND DISCUSSION

In this paper we have investigated how the latest cosmic shear data set, the CFHT weak lensing survey, can constrain neutrino masses. The weak lensing correlations can probe clustering strengths of total matter free of galaxy bias uncertainty, therefore, it allows us to explore the suppression signal in the weak lensing amplitudes caused by the free-streaming effect of finite-mass neutrinos. Since the measured shear correlation functions do not have strong features in the angular dependence, the shear amplitudes carry most of cosmological information. However, due to the limited information for the current data sets, the shear amplitudes integrated over a range of source galaxy redshifts are only available: the redshift dependence of the shear signals is not. For these reasons, constraining neutrino masses from the weak lensing data alone suffers from severe degeneracies among cosmological parameters such as $\sum m_\nu$, Ω_{m0} and the power spectrum normalization all of which are sensitive to overall amplitudes of the shear signals. Yet, interestingly enough, the neutrino mass constraint can be significantly improved when the weak lensing constraint is combined with other cosmological probes such as WMAP5, SNe and BAO, because the combination of these data sets helps efficiently break parameter degeneracies. The upper limits on the total neutrino mass found in this work are summarized as $\sum m_\nu < 1.1$ eV (WL+WMAP5), 0.76 eV (WMAP5+SNe+BAO), 0.54 eV (WL+WMAP5+SNe+BAO) at 95% confidence level, respectively. Note that we could not find any strong evidence of the lower limit for neutrino masses, i.e. a detection of the neutrino mass. This might be attributed to insufficient statistical precisions of the current data set (~ 30 square degrees).

Throughout this paper we have assumed a minimal cosmological model: a concordance Λ CDM model plus one additional parameter of the total neutrino mass. Thus our approach derives the best-available constraint on the neutrino mass from the weak lensing data combined with other cosmological probes. The constraint will be relaxed if additional parameters are included. In particular, dark energy equation of state parameter ($w \equiv p_{\text{de}}/\rho_{\text{de}}$) may be most intriguing to include, because a change in the equation of state from the cosmological constant ($w = -1$) does change the cosmic shear correlations in the shape and amplitude [34]. The cosmological constraints from the geometrical probes, SNe and BAO, are also relaxed if including w as a free parameter. Therefore the accuracy of the neutrino mass constraint is degraded if w is included as a free parameter. This is beyond the scope of this paper, and will be presented elsewhere.

Various weak lensing surveys are being planned and proposed so as to have a much increased survey area by a

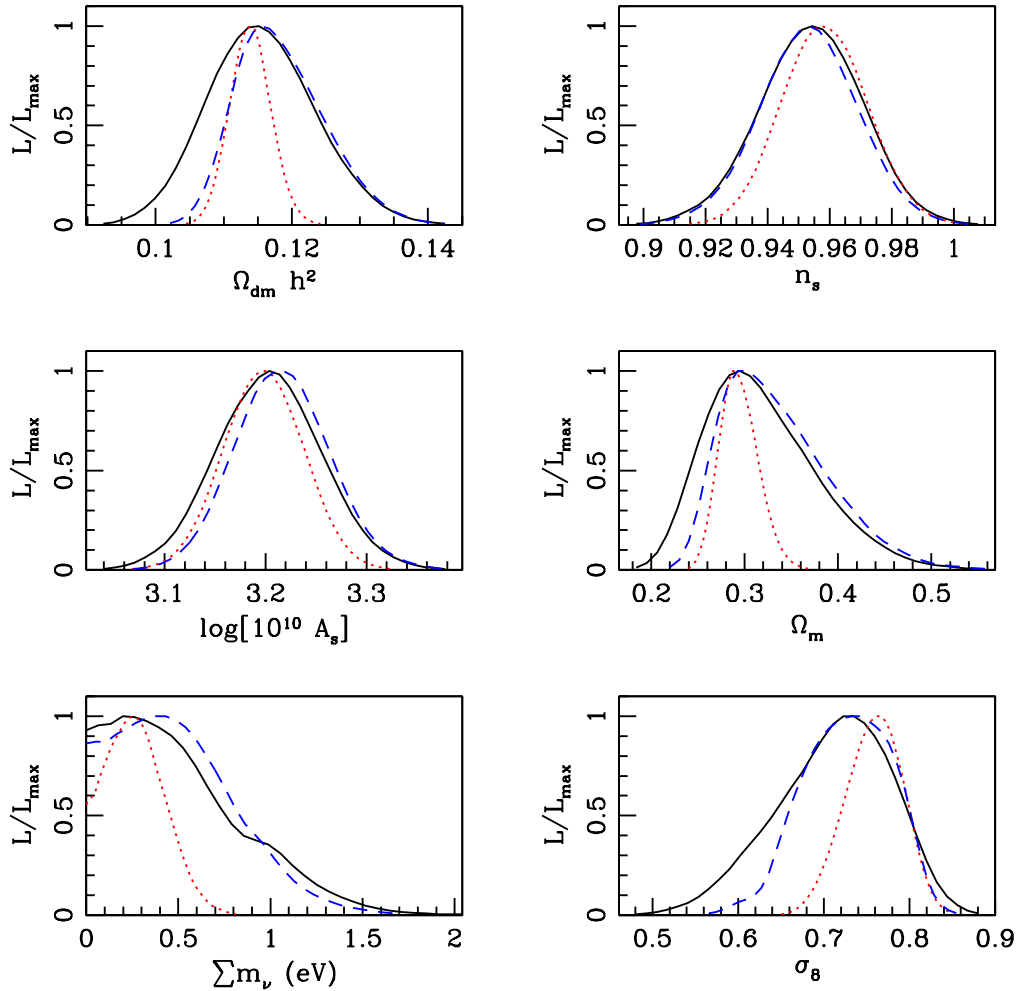


FIG. 8: One-dimensional marginalized likelihood on individual cosmological parameter for WMAP5 alone (solid curve), WL+WMAP5 (blue dashed) and WL+WMAP5+BAO+SNe (red dotted), respectively. Some of parameters, Ω_{m0} , $\Omega_{dm0}h^2$, σ_8 and $\sum m_\nu$, are significantly improved by combining all the probes, where those parameters are sensitive to the overall amplitudes of cosmic shear correlations.

factor of 100 compared to the CFHT survey, corresponding to a survey with area more than a few thousands square degrees. These surveys will promise to drastically improve the statistical accuracies of the cosmic shear measurements by a factor of 10 at each angular bins. Our results of Table I imply that such a survey may allow a precision of constraining the neutrino masses at level $\sigma(\sum m_\nu) \sim 0.8$ eV with the weak lensing data alone, if systematic errors inherent in the measurements are well under control. Combining with other probes allows to further improve the neutrino mass constraint as demonstrated in this paper. In addition, if multi-color information is available for future surveys as proposed, photometric redshift information is available to estimate the redshift distribution of source galaxies in a more reliable fashion. This additional redshift information is extremely useful in that it enables to recover redshift dependence of the lensing signals, the so-called lensing tomography, allowing to efficiently break parameter degeneracies such as σ_8 - Ω_{m0} degeneracy with the weak lensing data alone [34]. Therefore, if lensing tomography is available, weak lensing (combined with CMB and others) would potentially allow a detection of the neutrino masses.

In addition to the weak lensing technique, several cosmological probes have been proposed to constrain neutrino masses at accuracies of $O(0.1)$ eV, such as CMB lensing [58], 21cm experiments [59], galaxy surveys [8], cluster number count [60], and so on. All of these techniques are essentially based on the same effects of neutrinos, i.e., neutrinos suppress the power of density fluctuations on small scales. Therefore, these experiments including weak lensing allow us to make cross-checks of the cosmological constraint and hopefully to detect the finite mass of neutrinos, resolving

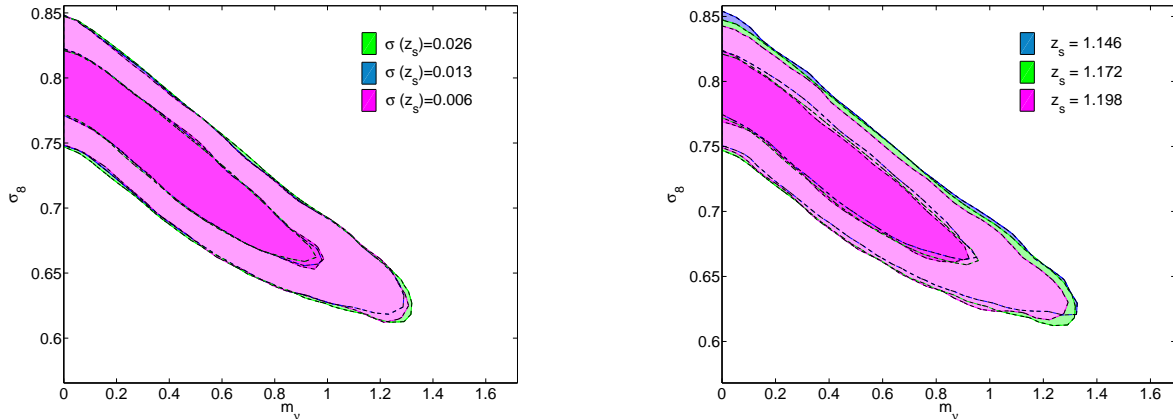


FIG. 9: Effects of possible residual uncertainties in the mean redshift of weak lensing galaxies on the cosmological constraints on $(\sum m_\nu, \sigma_8)$ for WL+WMAP5. The mean redshift is parametrized by z_s in Eqn. (2), and the parameter is calibrated as $z_s = 1.172 \pm 0.026$ according to [33]. We have so far assumed the Gaussian prior of $\sigma(z_s) = 0.026$ around the central value in the parameter estimations. *Left panel:* Shown is how the accuracy of the parameter estimation is changed if we assume a more restrict prior by a factor of 2 and 4 than the fiducial prior. The difference is indistinguishable, implying that this error is negligible compared to the measurement errors in shear correlations. *Right panel:* The effect of a shift in the central value of z_s on the parameter constraints: the green and red contours show the results obtained when the central value of z_s is changed by about 1σ statistical uncertainty to $z_s = 1.146$ and 1.198 , respectively. The difference is very small.

the hierarchy of neutrino masses with cosmological data sets.

When this paper was under completion, similar works for constraining the neutrino mass with the CFHT data combined with other cosmological probes were put forward by [61, 62]. In [61], they found an upper bound on neutrino masses which is consistent with ours. However, they also reported a lower bound $\sum m_\nu > 0.03$ eV which we could not find here. The difference may be attributed to different data set used for BAO and SNIa, and different covariance matrices from ours. In [62] they derived a constraint on neutrino masses from CFHT data without combining WMAP5 data. Therefore their obtained upper bound is slightly weaker than ours but it is a consistent result. After we submitted our paper, a similar paper [63] was posted on the arXiv, in which further data set such as SDSS LRG and the other CMB data were used to obtain the upper bound on neutrino masses.

Acknowledgments

We would like to thank K. Ichikawa, B. Jain, A. Kusaka, S. Saito and A. Taruya for useful discussion. This work was in part supported by World Premier International Research Center Initiative (WPI Initiative), MEXT, Japan, by Grant-in-Aid for Scientific Research on Priority Area No. 467 “Probing Dark Energy through an Extremely Wide and Deep Survey with Subaru Telescope”, by Grant-in-Aid for Scientific Research Grant (Nos. 17740129, 18072001, 19740145 and 20740119), by the Sumitomo Foundation, by Grant-in-Aid for the Global Center of Excellence program “Quest for Fundamental Principles in the Universe” at Nagoya University, as well as by Grant-in-Aid for the 21st Century Center of Excellence program “Exploring New Science by Bridging Particle-Matter Hierarchy” at Tohoku University.

-
- [1] T. Schwetz, M. Tórtola, and J. W. F. Valle, *New Journal of Physics* **10**, 113011 (2008), 0808.2016.
 - [2] E. W. Otten and C. Weinheimer, *Rept. Prog. Phys.* **71**, 086201 (2008).
 - [3] S. R. Elliott and P. Vogel, *Annual Review of Nuclear and Particle Science* **52**, 115 (2002), arXiv:hep-ph/0202264.
 - [4] P. Vogel, *ArXiv e-prints* (2008), 0807.2457.
 - [5] J. Lesgourgues and S. Pastor, *Phys. Rep.*, **429**, 307(2006), arXiv:astro-ph/0603494.
 - [6] J. R. Bond, G. Efstathiou, and J. Silk, *Physical Review Letters* **45**, 1980 (1980).
 - [7] W. Hu, D. J. Eisenstein, and M. Tegmark, *Physical Review Letters* **80**, 5255 (1998), arXiv:astro-ph/9712057.
 - [8] M. Takada, E. Komatsu, and T. Futamase, *Phys. Rev. D* **73**, 083520 (2006), arXiv:astro-ph/0512374.

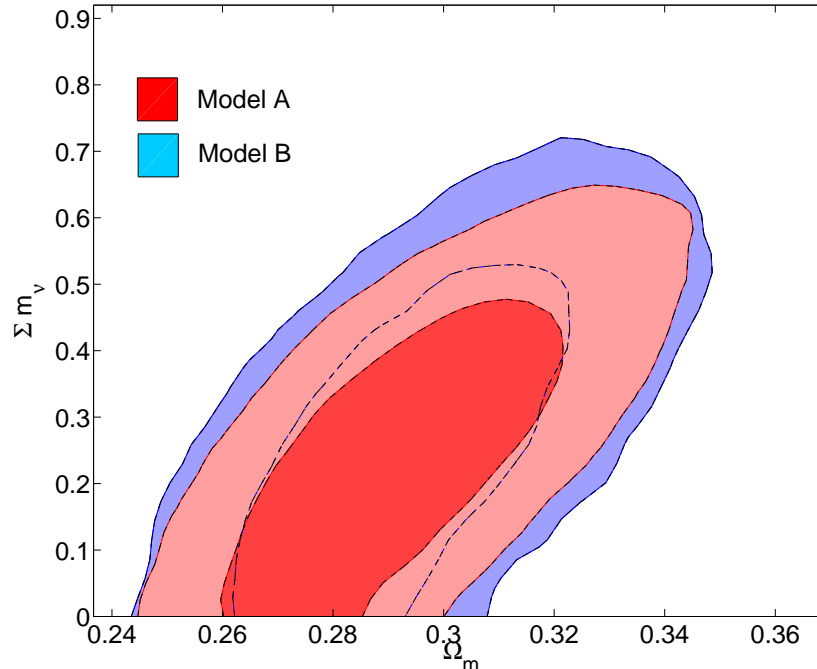


FIG. 10: Effects of possible uncertainties in non-Gaussian errors of the shear correlation covariances on the parameter constraints, for the $(\sum m_\nu, \Omega_{m0})$ -subspace. Note that we consider the combined constraints of WL+WMAP5+SNe+BAO. The red contours show the results when the halo model approach to compute the covariance (Model A: our fiducial model) is employed, while the blue contours show the results when the method developed in Semboloni et al. [46] is employed (Model B). Model B predicts stronger non-Gaussian errors than Model A, resulting in larger confidence regions in these parameter space. The best-fitting parameters are almost identical between these two models.

- [9] K. Ichikawa, M. Fukugita, and M. Kawasaki, *Phys. Rev. D* **71**, 043001 (2005), arXiv:astro-ph/0409768.
- [10] M. Fukugita, K. Ichikawa, M. Kawasaki, and O. Lahav, *Phys. Rev. D* **74**, 027302 (2006), astro-ph/0605362.
- [11] E. Komatsu, J. Dunkley, M. R. Nolta, C. L. Bennett, B. Gold, G. Hinshaw, N. Jarosik, D. Larson, M. Limon, L. Page, et al., *ArXiv e-prints* **803** (2008), 0803.0547.
- [12] M. Tegmark, D. J. Eisenstein, M. A. Strauss, D. H. Weinberg, M. R. Blanton, J. A. Frieman, M. Fukugita, J. E. Gunn, A. J. S. Hamilton, G. R. Knapp, et al., *Phys. Rev. D* **74**, 123507 (2006), arXiv:astro-ph/0608632.
- [13] C. J. MacTavish, P. A. R. Ade, J. J. Bock, J. R. Bond, J. Borrill, A. Boscaleri, P. Cabella, C. R. Contaldi, B. P. Crill, P. de Bernardis, et al., *Astrophys. J.* **647**, 799 (2006), arXiv:astro-ph/0507503.
- [14] J. R. Kristiansen, Ø. Elgarøy, and H. Dahle, *Phys. Rev. D* **75**, 083510 (2007), arXiv:astro-ph/0611761.
- [15] U. Seljak, A. Slosar, and P. McDonald, *Journal of Cosmology and Astro-Particle Physics* **10**, 14 (2006), arXiv:astro-ph/0604335.
- [16] S. Gratton, A. Lewis, and G. Efstathiou, *Phys. Rev. D* **77**, 083507 (2008), 0705.3100.
- [17] F. de Bernardis, P. Serra, A. Cooray, and A. Melchiorri, *Phys. Rev. D* **78**, 083535 (2008), 0809.1095.
- [18] M. Bartelmann and P. Schneider, *Phys. Rep.*, **340**, 291(2001), arXiv:astro-ph/9912508.
- [19] D. J. Bacon, A. R. Refregier, and R. S. Ellis, *MNRAS*, **318**, 625(2000), arXiv:astro-ph/0003008.
- [20] N. Kaiser, G. Wilson, and G. A. Luppino, *ArXiv Astrophysics e-prints* (2000), arXiv:astro-ph/0003338.
- [21] D. M. Wittman, J. A. Tyson, D. Kirkman, I. Dell'Antonio, and G. Bernstein, *Nature (London)* **405**, 143 (2000), arXiv:astro-ph/0003014.
- [22] L. Van Waerbeke, Y. Mellier, T. Erben, J. C. Cuillandre, F. Bernardeau, R. Maoli, E. Bertin, H. J. Mc Cracken, O. Le Fèvre, B. Fort, et al., *A&A*, **358**, 30(2000), arXiv:astro-ph/0002500.
- [23] A. R. Cooray, *A&A*, **348**, 31(1999), arXiv:astro-ph/9904246.
- [24] K. Abazajian and S. Dodelson, *Physical Review Letters* **91**, 041301 (2003), arXiv:astro-ph/0212216.
- [25] Y.-S. Song and L. Knox, *Phys. Rev. D* **70**, 063510 (2004), arXiv:astro-ph/0312175.
- [26] S. Hannestad, H. Tu, and Y. Y. Wong, *Journal of Cosmology and Astro-Particle Physics* **6**, 25 (2006), arXiv:astro-ph/0603019.
- [27] L. Fu, E. Semboloni, H. Hoekstra, M. Kilbinger, L. van Waerbeke, I. Tereno, Y. Mellier, C. Heymans, J. Coupon, K. Benabed, et al., *A&A*, **479**, 9(2008), arXiv:0712.0884.

- [28] G. Hinshaw, J. L. Weiland, R. S. Hill, N. Odegard, D. Larson, C. L. Bennett, J. Dunkley, B. Gold, M. R. Greason, N. Jarosik, et al., ArXiv e-prints (2008), 0803.0732.
- [29] M. Kowalski, D. Rubin, G. Aldering, R. J. Agostinho, A. Amadon, R. Amanullah, C. Balland, K. Barbary, G. Blanc, P. J. Challis, et al., *Astrophys. J.* **686**, 749 (2008), 0804.4142.
- [30] D. J. Eisenstein, I. Zehavi, D. W. Hogg, R. Scoccimarro, M. R. Blanton, R. C. Nichol, R. Scranton, H.-J. Seo, M. Tegmark, Z. Zheng, et al., *Astrophys. J.* **633**, 560 (2005), arXiv:astro-ph/0501171.
- [31] M. Takada and B. Jain, ArXiv e-prints (2008), 0810.4170.
- [32] O. Ilbert, S. Arnouts, H. J. McCracken, M. Bolzonella, E. Bertin, O. Le Fèvre, Y. Mellier, G. Zamorani, R. Pellò, A. Iovino, et al., *A&A*, **457**, 841(2006), arXiv:astro-ph/0603217.
- [33] O. Doré, M. Martig, Y. Mellier, M. Kilbinger, J. Benjamin, L. Fu, H. Hoekstra, M. Schultheis, E. Semboloni, and I. Tereno, ArXiv e-prints **712** (2007), 0712.1599.
- [34] M. Takada and B. Jain, *MNRAS*, **348**, 897(2004), arXiv:astro-ph/0310125.
- [35] R. E. Smith, J. A. Peacock, A. Jenkins, S. D. M. White, C. S. Frenk, F. R. Pearce, P. A. Thomas, G. Efstathiou, and H. M. P. Couchman, *MNRAS*, **341**, 1311(2003), arXiv:astro-ph/0207664.
- [36] A. Lewis, A. Challinor, and A. Lasenby, *Astrophys. J.* **538**, 473 (2000), astro-ph/9911177.
- [37] W. Hu and D. J. Eisenstein, *Astrophys. J.* **498**, 497 (1998), arXiv:astro-ph/9710216.
- [38] D. Huterer, *Phys. Rev. D* **65**, 063001 (2002), arXiv:astro-ph/0106399.
- [39] S. Saito, M. Takada, and A. Taruya, *Physical Review Letters* **100**, 191301 (2008), arXiv:0801.0607.
- [40] Y. Y. Y. Wong, *Journal of Cosmology and Astro-Particle Physics* **10**, 35 (2008), 0809.0693.
- [41] J. Brandbyge, S. Hannestad, T. Haugbølle, and B. Thomsen, *Journal of Cosmology and Astro-Particle Physics* **8**, 20 (2008), 0802.3700.
- [42] J. A. Peacock and S. J. Dodds, *MNRAS*, **280**, L19(1996), arXiv:astro-ph/9603031.
- [43] P. Schneider, L. van Waerbeke, and Y. Mellier, *A&A*, **389**, 729(2002), arXiv:astro-ph/0112441.
- [44] U.-L. Pen, L. Van Waerbeke, and Y. Mellier, *Astrophys. J.* **567**, 31 (2002), arXiv:astro-ph/0109182.
- [45] R. G. Crittenden, P. Natarajan, U.-L. Pen, and T. Theuns, *Astrophys. J.* **568**, 20 (2002), arXiv:astro-ph/0012336.
- [46] E. Semboloni, L. van Waerbeke, C. Heymans, T. Hamana, S. Colombi, M. White, and Y. Mellier, *MNRAS*, **375**, L6(2007), arXiv:astro-ph/0606648.
- [47] T. Eifler, M. Kilbinger, and P. Schneider, *A&A*, **482**, 9(2008), 0708.4125.
- [48] P. Schneider, L. van Waerbeke, M. Kilbinger, and Y. Mellier, *A&A*, **396**, 1(2002), arXiv:astro-ph/0206182.
- [49] A. J. S. Hamilton, C. D. Rimes, and R. Scoccimarro, *MNRAS*, **371**, 1188(2006), arXiv:astro-ph/0511416.
- [50] A. Kosowsky, M. Milosavljevic, and R. Jimenez, *Phys. Rev. D* **66**, 063007 (2002), arXiv:astro-ph/0206014.
- [51] A. Lewis and S. Bridle, *Phys. Rev. D* **66**, 103511 (2002), arXiv:astro-ph/0205436.
- [52] A. Gelman and D. Rubin, *Statistical Science* **7**, 457 (1992).
- [53] S. Dodelson, E. Gates, and A. Stebbins, *Astrophys. J.* **467**, 10 (1996), arXiv:astro-ph/9509147.
- [54] P. J. E. Peebles and J. T. Yu, *Astrophys. J.* **162**, 815 (1970).
- [55] W. Hu and N. Sugiyama, *Astrophys. J.* **471**, 542 (1996), arXiv:astro-ph/9510117.
- [56] W. J. Percival, S. Cole, D. J. Eisenstein, R. C. Nichol, J. A. Peacock, A. C. Pope, and A. S. Szalay, *MNRAS*, **381**, 1053(2007), arXiv:0705.3323.
- [57] T. Hamana, S. Miyazaki, K. Shimasaku, H. Furusawa, M. Doi, M. Hamabe, K. Imi, M. Kimura, Y. Komiyama, F. Nakata, et al., *Astrophys. J.* **597**, 98 (2003), arXiv:astro-ph/0210450.
- [58] J. Lesgourgues, L. Perotto, S. Pastor, and M. Piat, *Phys. Rev. D* **73**, 045021 (2006), arXiv:astro-ph/0511735.
- [59] M. McQuinn, O. Zahn, M. Zaldarriaga, L. Hernquist, and S. R. Furlanetto, *Astrophys. J.* **653**, 815 (2006), arXiv:astro-ph/0512263.
- [60] S. Wang, Z. Haiman, W. Hu, J. Khoury, and M. May, *Physical Review Letters* **95**, 011302 (2005), arXiv:astro-ph/0505390.
- [61] I. Tereno, C. Schimd, J.-P. Uzan, M. Kilbinger, F. H. Vincent, and L. Fu, ArXiv e-prints (2008), 0810.0555.
- [62] Y. Gong, T.-J. Zhang, T. Lan, and X.-L. Chen, ArXiv e-prints (2008), 0810.3572.
- [63] H. Li, J. Liu, J.-Q. Xia, L. Sun, Z.-H. Fan, C. Tao, A. Tilquin, and X. Zhang, ArXiv e-prints (2008), 0812.1672.
- [64] <http://lambda.gsfc.nasa.gov/>